Journal of Applied Microbiology

Journal of Applied Microbiology ISSN 1364-5072

ORIGINAL ARTICLE

Biosynthesis of zinc oxide nanoparticles with antimicrobial, anticancer, antioxidant and photocatalytic activities by the endophytic *Alternaria tenuissima*

H.K. Abdelhakim[1], E.R. El-Sayed[2] and F.B. Rashidi[3]

1 Biochemistry Lab, Chemistry Department, Faculty of Science, Cairo University, Giza, Egypt
2 Plant Research Department, Nuclear Research Center, Atomic Energy Authority, Cairo, Egypt
3 Chemistry Department, Faculty of Science, Cairo University, Giza, Egypt

Keywords
Alternaria tenuissima, anticancer, antimicrobial, antioxidant, photocatalytic, zinc oxide nanoparticles.

Correspondence
El-Sayed R. El-Sayed, Plant Research Department, Nuclear Research Center, Atomic Energy Authority, Cairo, Egypt.
E-mail: sayed_zahran2000@yahoo.com; elsayed.ramadan@eaea.org.eg

2019/2059: received 13 November 2019, revised 2 January 2020 and accepted 12 January 2020

doi:10.1111/jam.14581

Abstract

Aims: Zinc oxide nanoparticles (ZnONPs) were successfully synthesized using the culture filtrate of the endophytic fungus *Alternaria tenuissima* as a rapid, eco-friendly and cost-effective method.

Methods and Results: The rapid synthesis of ZnONPs was completed after 20 min as confirmed by UV–Vis spectroscopy. The synthesized ZnONPs showed a single-phase crystalline structure. Dynamic light scattering analysis showed that the synthesized ZnONPs were monodispersed and the recorded polydispersity index value was 0·311. Zeta potential value of −23·92 mV indicated the high stability of ZnONPs. Transmission electron microscope revealed the spherical shape and the mean particle size was 15.45 nm. Functional groups present in the prepared samples of ZnONPs were confirmed by Fourier transform infrared spectroscopy. Additionally, the biological activities of *in vitro* antimicrobial, anticancer, antioxidant as well as the photocatalytic activities were evaluated. ZnONPs showed broad spectrum of antimicrobial potential against all the tested plant and human pathogens. Based on the MTT assay, ZnONPs inhibited the proliferation of normal human melanocytes, human breast and liver cancer cell lines with IC_{50} concentrations of 55·76, 18·02 and 16·87 μg ml^{-1}. ZnONPs exhibited promising antioxidant potential with 50% inhibitory concentration of 102·13 μg ml^{-1}. Moreover, ZnONPs showed efficient degradation of methylene blue dye.

Conclusions: The synthesized ZnONPs showed promising activities that can be better explored in the near future for many medical, agricultural and industrial applications.

Significance and Impact of the Study: This study suggests a new and alternate approach with the excellent biotechnological potentiality for the production of ZnONPs which could open up the way for the industrial manufacture of nanoparticles using microbial platforms.

Introduction

Zinc (Zn) is one of the most important essential elements for animals, human and micro-organisms. Zn has a key role in maintaining crucial cellular processes including DNA replication, oxidative stress, DNA repair and cell cycle progression (Bisht and Rayamajhi 2016). Recently, zinc oxide nanoparticles (ZnONPs) have gained tremendous attention due to their unique properties. ZnONPs had high absorption rate, lower toxicity (Yusof *et al.* 2019), better bioavailability and biocompatibility compared to their conventional Zn sources (Hosseini and

Sarviab 2015; Shahid *et al.* 2019). They showed a wide range of biological and therapeutic activities including antibacterial (Shahid *et al.* 2018; Abd Elkodous *et al.* 2019), antioxidant (Gao *et al.* 2019), antiprotozoa (Wajiha *et al.* 2018) and anticancer (Bisht and Rayamajhi 2016). In addition, recent studies indicated the promising properties of ZnONPs that could be implemented in the poultry and livestock industry (Zhao *et al.* 2014; Khoobbakht *et al.* 2018). As such, ZnONPs are gaining great importance in the field of optics and electronics due to their enhanced semiconducting (Sharma *et al.* 2011), photoelectrical (Udayabhanu *et al.* 2016) and catalytic properties (Kalpana *et al.* 2018; Khan *et al.* 2018). Such activities make ZnONPs ideal candidates for many industrial and medical applications. Traditionally, the synthesis of ZnONPs is performed by a variety of chemical and physical methods (Abd Elkodous *et al.* 2019). These methods are complicated, costly and result in hazardous toxic wastes, which are harmful to both the human health and environment. Moreover, the toxic chemicals required in such methods greatly reduce their biomedical applications (Yusof *et al.* 2019). So, there is a pressing scientific need to explore alternative green sources to overcome these drawbacks. In green synthesis of metal nanoparticles, the difficult task is to find a suitable and nontoxic natural product, as well as an eco-friendly solvent system (Ljaz *et al.* 2017). The microbial synthesis of nanoparticles has its own advantages over plant-mediated synthesis since microbes are easily reproduced.

In comparison with other microbes, fungi could be used as the most efficient biotechnology agents for the sustainable production of nanoparticles. Fungi are flexible, tolerant, easy and economic biological system that has been used extensively in the industry (Dorcheh and Vahabi 2016). Among the fungal populations, endophytic fungi are a group of fungi which spend their whole or part of their lifecycle colonizing the inside of healthy tissues of the host plants, typically causing no apparent symptoms of disease (Ismaiel *et al.* 2017). Endophytic fungi represent an untapped pool of valuable metabolites (El-Sayed *et al.* 2019a, 2019b; Zaki *et al.* 2019). Moreover, they are metabolically more active than their free counterparts; so, they are recognized as sources of novel metabolites with potential application in agriculture, medicine and food industry (El-Sayed *et al.* 2019c, 2020c).

Till now, the microbial synthesis of ZnONPs still remains unexplored. Few reports have demonstrated the microbial synthesis of ZnONPs using some bacterial, yeast, and fungal strains. Furthermore, data regarding the production of ZnONPs using fungi is in rare; only few fungal genera were reported to synthesize these nanoparticles (Yusof *et al.* 2019). Additionally, a simple and reproducible method for the production of ZnONPs on a large scale is still missing. Thus, developing a simple, cost-effective and eco-friendly preparation method for ZnONPs becomes essential. As a first step in this direction, the synthesis and characterization of ZnONPs using the endophytic fungus *Alternaria tenuissima* was described for the first time. Biological applications of the antimicrobial, anticancer and antioxidant potentials of the synthesized nanoparticles were evaluated. Moreover, the photocatalytic activities of the synthesized nanoparticles were also studied.

Materials and methods

Fungal strain

The experimental fungus used in this study was *A. tenuissima* AUMC10624 (Culture Collection of Assiut University Mycological Center, Assiut, Egypt, http://www.aun.edu.eg/aumc/aumc.htm). The fungus was routinely maintained on malt extract agar composed of (g l^{-1}): malt extract 20, glucose 20, agar 20 and peptone 1·0. The fungus was stored in glycerol (15%, v/v) at −4°C, as a suspension of mycelium and spores.

Preparation of *A. tenuissima* cell-free culture filtrate

Fungal spores from the cultures (7 days old) of *A. tenuissima* were harvested and the spore concentration was adjusted to a concentration of 10^6 spores per ml. Potato-dextrose broth was prepared and the pH was adjusted to 6·0. About 50 ml aliquots of the broth were transferred to 250 ml Erlenmeyer flasks and then sterilized, cooled and inoculated with 1 ml of the fungal spore suspension after which, the inoculated flasks were incubated under static conditions for 10 days at 30°C. Finally, the inoculated flasks were filtered through Whatman no. 1 filter paper at the end of incubation and the filtrate was used for the preparation of nanoparticles.

Synthesis of ZnONPs

Zinc sulphate ($ZnSO_4 \cdot 7H_2O$) was purchased from Sigma-Aldrich (St. Louis, MO). A volume of 100 ml of the *A. tenuissima* cell-free culture filtrate (ATCF) was taken in an Erlenmeyer flask and mixed with 100 ml of the zinc sulphate (2 mmol l^{-1} final concentration). The reaction mixture was maintained under vigorous stirring for 20 min at room temperature and the mixture was observed visually for formation of white precipitate. The precipitate (ZnONPs) was separated by ultracentrifugation for 20 min at 20 000 rev min^{-1} after which, the separated nanoparticles were washed in deionized water and ethanol and then dried at 50°C in a hot air oven. Finally, the fine

powder of ZnONPs was dissolved in ethanol (HPLC grade) and treated ultrasonically for the dispersion of the individual nanoparticles and used for characterization.

Characterization of ZnONPs

The synthesized nanoparticles were characterized by various techniques. ZnONPs synthesized by the cell-free filtrate of *A. tenuissima* were confirmed by UV–Vis spectroscopy. ZnONPs solution was analysed on UV–Vis spectrophotometer (UV-3101PC; Shimadzu, Kyoto, Japan). X-ray diffraction (XRD) pattern was recorded using Cu-Kα radiation (wavelength of 1·5406°A at 40 kV and 40 mA) in the range $20° \leq 2\Theta \leq 80°$ through a BRUKER diffractometer (D8 DISCOVER with DAVINCI design, Billerica, MA, USA). Dynamic light scattering (DLS) and Zeta potential analyses (Zetasizer Nano ZS; Malvern Instruments, Worcestershire, UK) were carried out to estimate the distribution of different size particles dispersed in ZnONPs solution and its stability. Morphology of the synthesized nanoparticles was studied by Transmission Electron Microscope (TEM) performed on a JOEL model 2100, Japan, operated at an accelerating voltage at 8000 kV by focusing on nanoparticles. Fourier transform infrared (FTIR) spectra were recorded at 400–4000 cm^{-1} using IRAffinity-1 spectrophotometer (Shimadzu).

In vitro antimicrobial sensitivity tests

ZnONPs were dissolved in different volumes of methanol (HPLC grade) to obtain the desired concentrations of 50, 100, 200 and 400 μg ml^{-1} and then treated ultrasonically. Antimicrobial activity assay was performed using agar well diffusion assay technique (Pongtharangkul and Demirci 2004).

Antibacterial activity

Antibacterial susceptibility assay of ZnONPs was performed against different Gram negative and Gram positive bacterial strains (*Pseudomonas aeruginosa* ATCC 15442, *Klebsiella pneumoniae* ATCC 13883, *Escherichia coli* ATCC 11229 and *Staphylococcus aureus* ATCC 6538). ZnONPs (50 μl) were applied to agar wells (9 mm, diameter) in a Petri-dish containing 25 ml Muller–Hinton agar medium (composed of (g l^{-1}): beef infusion 300, acid hydrolysate of casein 17·5, starch 1·5 and agar 20) inoculated with 0·1 ml suspension (10^7 spores per ml) of the bacterial strains. Control Petri-dishes were made by applying methanol only (negative control) and amoxicillin/clavulanic acid (positive control) to the agar wells. Plates were incubated at 4°C overnight and then at 35°C for 24 h.

Antifungal activity

Antifungal potential of ZnONPs was evaluated against *Candida albicans* ATCC 10231 and three different plant pathogenic fungi (*Alternaria solani, Aspergillus niger* and *Fusarium oxysporum*). The fungal isolates are used as standard micro-organisms in our laboratory (Microbiology Research Unit, Plant Research Department, Nuclear Research Center, Egypt). Petri-dishes containing Czapek–Dox's agar (composition (g l^{-1}): sucrose 30, $NaNO_3$ 3, KH_2PO_4 1, $MgSO_4 \cdot 7H_2O$ 0·5, KCl 0·5, $FeSO_4 \cdot 7H_2O$ 0·01, agar, 20) inoculated with 0·2 ml spore suspension (10^7 spores per ml) of the tested fungal species was prepared. However, *C. albicans* (10^7 cell per ml) was cultured in Petri-dish containing 25 ml Sabouraud's-glucose agar composed of (g l^{-1}): bactopeptone 10, KH_2PO_4 1, glucose 20, $MgSO_4 \cdot 7H_2O$ 1 and agar 20. Control Petri-dishes were made by applying methanol only (negative control) and nystatin (positive control) to the agar wells. Plates were incubated at 4°C overnight and then at 35°C for 24 h for *C. albicans* or at 30°C for 5 days for the fungal species.

Inhibition zones around the agar wells were carefully measured. The wells containing the lowest concentration of ZnONPs that still showed a zone of inhibition were considered the minimum inhibitory concentration (MIC).

In vitro anticancer activity

Cell lines

Normal human melanocytes (HFB-4), hepatocelluar carcinoma (HepG-2) and human breast carcinoma (MCF-7) cell lines were obtained from The American Type Culture Collection ATCC (MO http://www.atcc.org). Cell lines were maintained by serial subculturing in Dulbecco's modified Eagle's medium supplemented with 10% bovine serum, 100 U ml^{-1} penicillin and 100 μg ml^{-1} streptomycin. The cells were subcultured every 3 days and maintained in a humidified incubator supplied with 5% CO_2 and temperature 37°C.

Cytotoxicity evaluation

The synthesized nanoparticles were dissolved in DMSO (HPLC grade) to a concentration range of 0·39–50 μg ml^{-1}. Taxol (Sigma-Aldrich) was used as a standard anticancer agent at the same concentrations of ZnONPs. The MTT (3-(4,5-dimethyl-2-thiazolyl)-2,5-diphenyl-2H tetrazolium bromide)-based assay was used to evaluate the cytotoxicity of ZnONPs against the cell lines (El-Sayed *et al.* 2020a). In brief, cell monolayers (10^4 cells per well) were incubated in a 5% CO_2 humidified incubator at 37°C for 24 h and then incubated for another 48 h and washed

by HEPES buffer (Lonza Bioproducts, Basel, Switzerland). Cells were treated with 50 µl of 0·5 mg ml^{-1} MTT (Serva Electrophores, GmbH, Heidelberg, Germany) added to each well after which, they were dark incubated for 4 h for the reduction of MTT into formazan followed by addition of 50 µl of DMSO to solubilize the purple crystals of formazan. Absorbance was finally recorded at 570 nm with a microplate ELISA reader (BioTek, Winooski, Vermont, USA). The untreated cells were used as control. Samples and control were treated in quadrates for each concentration of ZnONPs. The relative viability of cells (%) was expressed as follows:

$$\%\,\text{Cell viability} = (\text{Abs}_{570}\,\text{of treated cells}/\text{Abs}_{570}\,\text{of control cells}) \times 100.$$

The 50% inhibitory concentration (IC_{50}) was calculated from graphic plots for each concentration using the GraphPad Prism software.

In vitro antioxidant activity

Free radical scavenging potential of ZnONPs was estimated by 2,2′-diphenyle picrylhydrazyl (DPPH) radical scavenging assay (El-Sayed *et al.* 2020b). ZnONPs were dissolved in methanol (HPLC grade) and treated ultrasonically to get the concentrations of 25, 50, 100, 200, 400, 800 and 1000 µg ml^{-1}. A stock solution was prepared by dissolving 24 mg of DPPH (Sigma-Aldrich) in 100 ml of methanol and stored at −4°C. Then, 2 ml of the stock solution was added to 1 ml of ZnONPs solution. This mixture was dark incubated for 30 min and the final absorbance was recorded at 517 nm. Simultaneously, ascorbic acid (Sigma-Aldrich) was used as a positive control. The percentage scavenging activity is expressed as the change in absorbance with respect to the control (containing DPPH only). Moreover, the concentration required to reduce the free radicals by 50% (IC_{50}) was estimated from graphic plots for each concentration using GraphPad Prism software (San Diego, CA).

Photocatalytic activities

The photocatalyitc potential of the synthesized nanoparticles was evaluated in the degradation of methylene blue (MB) dye (Sigma-Aldrich) according to the method described by Udayabhanu *et al.* (2016) with slight modification. Different concentrations of the prepared ZnONPs powder (25, 50, 100, 200 and 400 mg) were separately added to 100 ml aqueous solution of MB (10 mg l^{-1}) under constant stirring for 1 h in the dark to attain the adsorption equilibrium. This mixture was then exposed to the sunlight at room temperature for 20 min after which, 10 ml of the aliquot was withdrawn from the ZnONPs-dye mixture, centrifuged and the absorbance were monitored by at 664 nm. A control experiment was carried out under the same condition without addition of nanoparticles. The percentage of dye degradation was estimated by the following equation:

$$\text{Degradation}\ (\%) = 100 \times (\text{Mo} - \text{M})/\text{Mo}$$

where Mo is the original concentration of MB and M is the MB concentration after catalytic degradation.

Statistical analyses

Results were expressed as the mean ± standard deviation (SD). The statistical significance was evaluated by the one-way ANOVA analysis followed by the least significant difference test at 0·05 level using SPSS software, ver. 22 (IBM Corp., NY).

Results

Synthesis and characterization of ZnONPs

The cell-free filtrate of *A. tenuissima* culture (Fig. 1a) was added to the aqueous colourless bulk zinc sulphate solution. After 20 min of incubation, a white precipitate was observed, indicating the complete reduction of zinc sulphate to ZnONPs (Fig. 1b). The UV–Vis spectrophotometric analysis was performed to confirm the formation of ZnONPs from zinc sulphate. In the UV–Vis spectrum (Fig. 1c), the synthesized ZnONPs exhibited an absorption peak at 369 nm, due to its surface plasmon resonance.

Table 1 presented the crystallographic data obtained by XRD analyses and Fig. 2 showed the XRD pattern of ZnONPs synthesized by the ATCF. The obtained results indicated that the crystal structure of the synthesized ZnONPs was hexagonal type with space group P36mc. Moreover, the presence of 100, 002, 101, 102, 110, 103, 220, 112 and 201 planes in the XRD pattern confirms the crystal structure. The synthesized ZnONPs showed a single phase, as no peaks corresponding to impurities were observed (Fig. 2). The obtained results further showed that the recorded lattice parameter was 0·323420 nm. The crystallite size of ZnONPs was estimated using the Scherrer equation (from the FWHM of the most intense peak corresponding to the 101 plane) as follows:

$$D = k\lambda/\beta \cos\theta,$$

where D, k, λ, β and θ are crystallite size, Scherrer constant, the wavelength of the X-ray, full width half-maximum of the (101) plane and Bragg diffraction angle respectively. The mean crystallite size of the synthesized

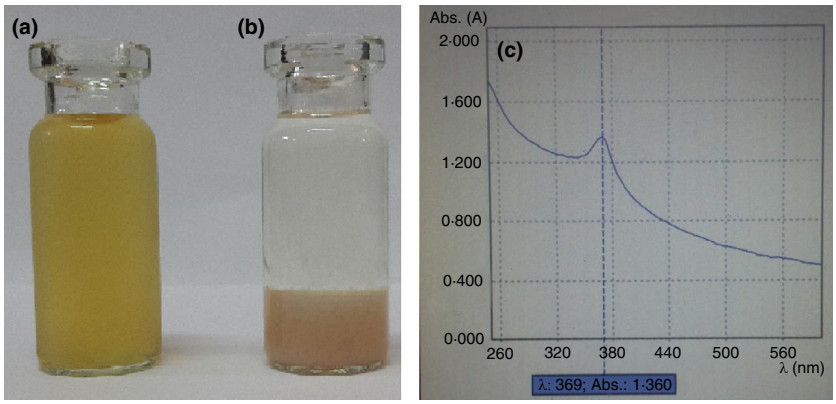

Figure 1 UV–Vis spectrum of ZnONPs synthesized by the ATCF. ZnONPs were dissolved in ethanol and treated ultrasonically for the dispersion of the individual particles and the absorption was recorded in the range of 200–800 nm. (a) *Alternaria tenuissima* culture filtrate, (b) Reaction mixture after complete reduction showing the formation of ZnONPs, and (c) UV–Vis spectrum of the synthesized ZnONPs.

Table 1 Crystallographic data of ZnONPs synthesized by the *Alternaria tenuissima* culture filtrate

Crystallographic data		XRD data	
Formula	ZnO	Temperature (°C)	25
Crystal system	Hexagonal	Wavelength (CuKa) (nm)	0·15406
Space group (n)	P 63 mc	Monochromator	Graphite
Lattice parameter (nm)	0·323420	Measuring range (°)	$20 \leq 2\theta \leq 80$
Cell volume (Å^3)	588·61	Step (°2θ)	0·011
Mean crystallite size (nm)	15·45	Integration time (s)	30

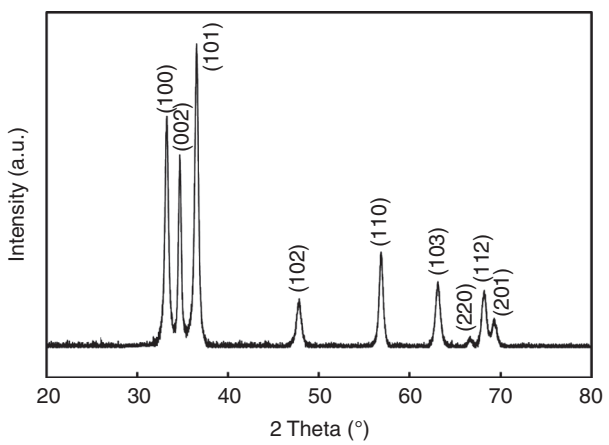

Figure 2 X-ray diffraction pattern (Cu Kα-radiation) of ZnONPs synthesized by the ATCF at room temperature.

ZnONPs was 15·45 nm (Table 1). The obtained results also revealed that the lattice parameter was 4·44690 Å.

Dynamic light scattering was used to estimate the size distribution of the synthesized ZnONPs. Data presented in Fig. 3a showed that the particles size distribution was in the range 10–30. The polydispersity index (PDI) value of the synthesized ZnONPs was 0·311, indicating that the

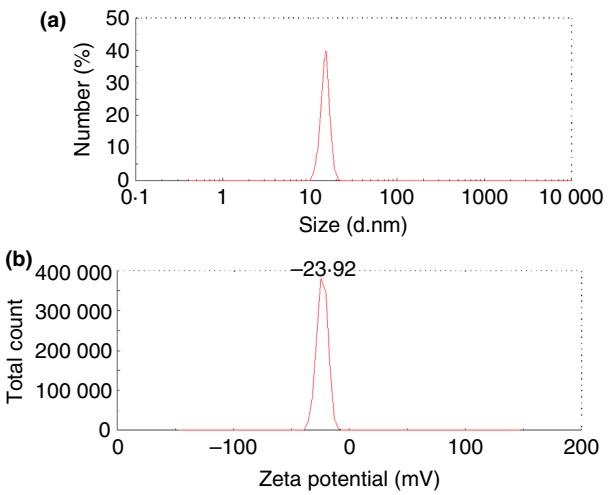

Figure 3 DLS analyses of ZnONPs synthesized by the *Alternaria tenuissima* culture filtrate; (a) Particle size distribution, and (b) Zeta potential.

synthesized nanoparticles were monodispersed. The zeta potential value (Fig. 3b) of the synthesized ZnONPs was −23·92 mV which indicated that the synthesized nanoparticles had high stability. TEM analysis was accomplished to study the morphology and particle-sized distribution of ZnONPs synthesized by the ATCF. TEM images of the synthesized ZnONPs (Fig. 4a) showed that the particles were spherical in shape. Moreover, SAED pattern (Fig. 4b) showed five distinct rings indexed to be the 100, 002, 101, 110 and 103 lattice planes. Figure 4c showed that the particle size distribution was in the range 10−30 nm and the mean particle size was 15·62 ± 4·51 nm.

Fourier transform infrared spectra were recorded to study the interaction between active metabolites of the ATCF and the synthesized ZnONPs. FTIR spectra (Fig. 5) of the synthesized nanoparticles and the ATCF were recorded in the 400–4000 cm^{-1} range. Both spectra showed main bands of C-H in CH_2 and in the phenyl ring, asymmetric and symmetric vibrations of C-O and C = O

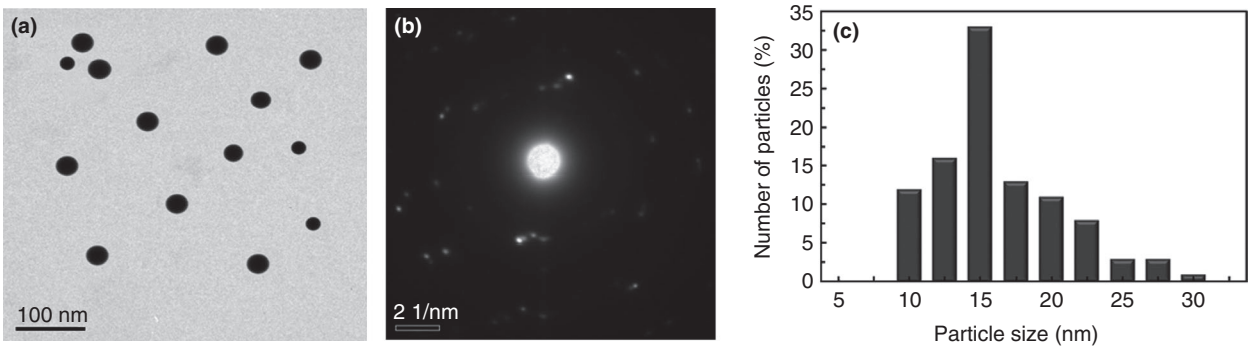

Figure 4 TEM analysis of ZnONPs synthesized by the *Alternaria tenuissima* culture filtrate; (a) TEM micrograph, (b) SAED pattern, (c) particle size distribution histogram.

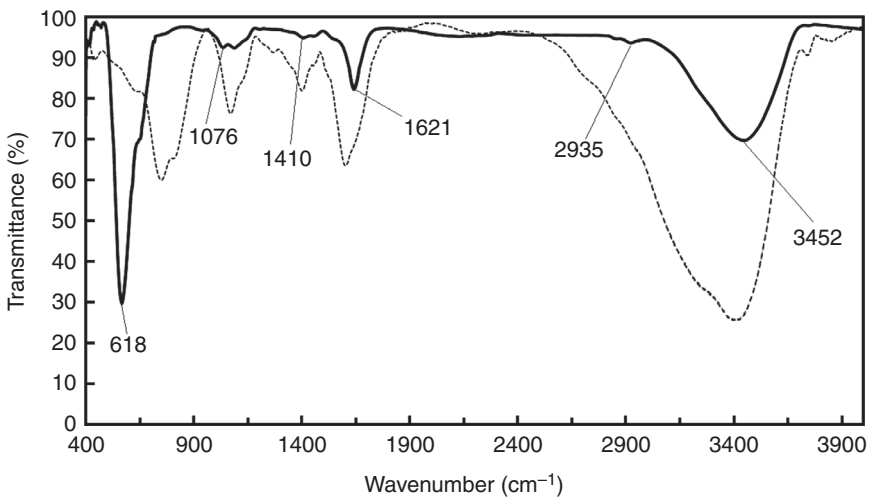

Figure 5 FTIR spectra of the *Alternaria tenuissima* culture filtrate (ATCF, dotted line) and the synthesized ZnONPs (solid line).

bonds in COO^- groups as well as bands of O-H in water. Besides, bands of phenols and primary amines were also detected. Interestingly, an absorption band at 618 cm^{-1} appeared in the recorded spectrum of ZnONPs, which may be due to conjugation of the synthesized nanoparticles. Figure 5 further indicated the presence of the COO^- groups and OH groups in the synthesized ZnONPs.

Antimicrobial activity of ZnONPs

The antimicrobial potential of the synthesized ZnONPs were evaluated against different Gram-positive and Gram-negative pathogenic bacterial strains as well as different plant pathogenic fungi and a unicellular fungal strain. Data presented in Table 2 clearly revealed that ZnONPs exhibited a broad spectrum antibacterial activity when compared with amoxicillin/clavulanic acid, where it inhibited growth of all the tested bacterial strains. The recorded results also clearly showed that the MIC value of the *P. aeruginosa, K. pneumoniae* and *S. aureus* was 200 μg ml^{-1} while for *E. coli* it was 100 μg ml^{-1}.

Results of the antifungal activity (Table 2) clearly indicated that ZnONPs showed potent antifungal potential against all the tested fungal species, as compared by the standard antifungal nystatin. The obtained results showed that the MIC values of the synthesized ZnONPs vary according to the employed fungal species. *C. albicans* was the most sensitive towards ZnONPs where the lowest concentration of 50 μg ZnONPs ml^{-1} resulted in an inhibition zone of 01·87 ± 0·06 mm. In the case of *A. solani* and *F. oxysporum*, the MIC value of ZnONPs was 100 μg ml^{-1}. However, the MIC value of ZnONPs was 200 μg ml^{-1} for *A. niger*.

Anticancer activity of ZnONPs

Table 3 showed that ZnONPs were active against the nonmalignant Hbf-4 cell line and both malignant MCF-7

Table 2 Antimicrobial activity of ZnONPs synthesized by the *Alternaria tenuissima* culture filtrate against different multidrug-resistant pathogenic bacterial strains, unicellular fungi and plant pathogenic fungi

	Diameter of inhibition zone (mm)					
Pathogen	50 (μg ml^{-1})	100 (μg ml^{-1})	200 (μg ml^{-1})	400 (μg ml^{-1})	Am/Clav	Nystatin
Escherichia coli	–	04·67 ± 0·11^{a}	16·55 ± 1·03^{b}	22·67 ± 1·06^{c}	08·65	–
Staphylococcus aureus	–	–	09·65 ± 0·63^{a}	20·87 ± 1·12^{b}	–	–
Pseudomonas aeruginosa	–	–	07·09 ± 0·51^{a}	18·57 ± 1·13^{b}	–	–
Klebsiella pneumoniae	–	–	14·78 ± 1·09^{a}	21·47 ± 1·15^{b}	–	–
Aspergillus niger	–	05·98 ± 0·15^{a}	17·89 ± 1·12^{a}	23·23 ± 1·12^{b}	–	–
Alternaria solani	–	–	09·51 ± 0·42^{a}	18·21 ± 1·15^{b}	–	–
Fusarium oxysporum	–	–	06·43 ± 0·35^{a}	16·21 ± 1·17^{b}	–	–
Candida albicans	01·87 ± 0·06^{a}	07·01 ± 0·21^{b}	13·57 ± 1·12^{c}	24·43 ± 1·25^{d}	–	10·65

Am/Clav, amoxicillin/clavulanic acid and nystatin were used at a concentration of 100 μg ml^{-1}. Calculated mean is for triplicate measurements from two independent experiments ± SD, $^{a–d}$means with different superscripts in the same row are considered statistically different (LSD test, $P \leq 0·05$).

Table 3 Anticancer activity of ZnONPs synthesized by the *Alternaria tenuissima* culture filtrate against Hepatocelluar carcinoma (HepG-2), human breast carcinoma (MCF-7) and normal human melanocytes (Hfb-4)

	Cell viability (%)					
	Hfb-4 (normal)		HepG-2 (liver)		MCF-7 (breast)	
Concentration (μg ml^{-1})	ZnONPs	Taxol	ZnONPs	Taxol	ZnONPs	Taxol
0·00 (C)	100·00 ± 0.0^{a}	100·00 ± 0.0^{a}	100·00 ± 0.0^{a}	100·00 ± 0.0^{a}	100·00 ± 0.0^{a}	100·00 ± 0.0^{a}
0·39	100·00 ± 0.0^{a}	99·34 ± 5·01^{a}	100·00 ± 0.0^{a}	96·52 ± 3·42^{a}	100·00 ± 0.0^{a}	99·67 ± 1·61^{a}
0·78	100·00 ± 0.0^{a}	98·76 ± 2·45^{a}	97·56 ± 1·87^{a}	81·96 ± 4·19^{b}	99·33 ± 3·21^{a}	92·37 ± 2·31^{b}
1·56	100·00 ± 0.0^{a}	87·43 ± 2·11^{b}	85·44 ± 3·51^{b}	75·68 ± 3·88^{c}	89·65 ± 3·21^{b}	81·57 ± 1·77^{c}
3·125	92·12 ± 3·67^{b}	72·55 ± 1·98^{c}	75·38 ± 2·51^{c}	68·81 ± 5·65^{d}	79·44 ± 4·27^{c}	72·61 ± 1·25^{d}
6·25	81·65 ± 1·57^{c}	60·84 ± 2·34^{d}	60·59 ± 2·79^{d}	53·96 ± 3·57^{e}	65·21 ± 4·52^{d}	59·43 ± 1·39^{e}
12·50	74·22 ± 1·87^{d}	50·11 ± 1·33^{e}	54·29 ± 1·59^{e}	48·07 ± 2·98^{f}	57·33 ± 5·33^{e}	46·68 ± 2·09^{f}
25·00	51·89 ± 1·36^{e}	44·42 ± 1·09^{f}	41·66 ± 2·17^{f}	39·67 ± 1·09^{g}	40·21 ± 3·21^{f}	39·55 ± 1·44^{g}
50·00	35·61 ± 1·08^{f}	37·75 ± 1·17^{g}	39·54 ± 1·08^{g}	31·21 ± 1·12^{h}	31·87 ± 2·65^{g}	21·89 ± 1·92^{h}
IC_{50} (μg ml^{-1})	55·76	12·05	16·87	10·35	18·02	10·42

MTT-based assay was used for measuring the cytotoxic activities of the synthesized ZnONPs at 570 nm using MTT solution under the conditions described in the Materials and Methods section, calculated mean is for triplicate measurements from two independent experiments ± SD, $^{a–h}$means with different superscripts in the same column are considered statistically different (LSD test, $P \leq 0·05$).

and HepG-2 cancer cell lines. In addition, the least inhibitory concentration of ZnONPs was found to vary from cell line type to another. The obtained results also revealed that ZnONPs exhibited a strong anticancer activity compared to Taxol. The least inhibitory concentration of the synthesized ZnONPs was 0·78 μg ml^{-1} against MCF-7 and HepG-2 cells, and 3·125 μg ml^{-1} against Hfb-4. However, the least inhibitory concentrations of taxol against these cell lines was 0·39 μg ml^{-1}. Data presented in Table 3 further showed that ZnONPs caused concentration-dependent cell death where the increase in ZnONPs' concentration resulted in a significant decrease in cell proliferation. The estimated IC_{50} values of the synthesized ZnONPs were 55·76, 16·87 and 18·02 μg ml^{-1} against Hfb-4 and HEp-2, MCF-7 respectively. Meanwhile, the estimated IC_{50} values of taxol against the respective cell lines were 12·50, 10·35 and 10·42 μg ml^{-1} (Table 3).

DPPH free radical scavenging activity of ZnONPs

Table 4 clearly showed that the synthesized ZnONPs exhibited promising antioxidant activity when compared by ascorbic acid as a standard antioxidant at different concentrations. The obtained results also confirmed that ZnONPs inhibited the DPPH-free radicals in a dose-dependent manner, as any increase in the ZnONPs concentration was followed by an increase in the recorded

Table 4 DPPH free radical scavenging activity of ZnONPs synthesized by the *Alternaria tenuissima* culture filtrate

	Free radical scavenging activity (%)	
Concentration (μg ml^{-1})	Ascorbic acid	ZnONPs
0·00 (C)	00·00 ± 0·00^{h}	00·00 ± 0·00^{g}
25	21·52 ± 0·65^{g}	18·37 ± 1·09^{f}
50	47·37 ± 2·31^{f}	39·76 ± 1·23^{e}
100	52·99 ± 1·57^{e}	50·92 ± 2·65^{d}
200	64·67 ± 2·44^{d}	68·51 ± 1·99^{c}
400	72·59 ± 2·29^{c}	78·61 ± 2·36^{b}
800	99·89 ± 1·55^{b}	85·33 ± 2·76^{a}
1000	100·00 ± 0·00^{a}	92·51 ± 2·96^{a}
IC_{50} (μg ml^{-1})	72·95	102·13

DPPH scavenging assay was used for measuring the antioxidant activities of ZnONPs at 517 nm using DPPH solution under conditions described in the Materials and Methods section. Calculated mean is for triplicate measurements from two independent experiments ± SD, $^{a–h}$means with different superscripts in the same column are considered statistically different (LSD test, $P \leq 0·05$).

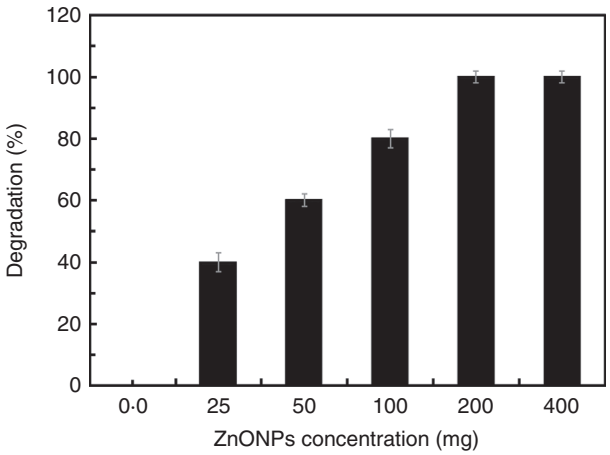

Figure 6 Effect of different concentrations (mg) of the synthesized ZnONPs on the degradation of MB dye under solar irradiation. All data are shown as the mean ± SD of triplicate measurements from two independent experiments.

scavenging activity (Table 4). Moreover, the least inhibitory concentration of both ZnONPs and ascorbic acid was 25 μg ml^{-1}. The obtained results also revealed that the recorded IC_{50} value of ZnONPs was 102·13 μg ml^{-1}, meanwhile, it was 72·95 μg ml^{-1} for ascorbic acid.

Photocatalytic activity of ZnONPs

The photocatalytic behaviour of the synthesized ZnONPs was examined through the degradation of MB dye after being left in dark for 1 h to attain equilibrium. The dye degradation in the presence of the synthesized ZnONPs was confirmed by the decrease in the recorded absorbance (at 664 nm) after 20-min exposure in sunlight. Degradation was verified by gradual change in the of MB colour from deep blue to colourless. Figure 6 presented the effect of different concentrations of ZnONPs on the degradation of MB dye. The obtained data revealed that the synthesized ZnONPs successfully degraded the MB dye in a concentration-dependent manner as shown in Fig. 6. A gradual increase in the per cent of degradation is achieved in association with the increase in the ZnONPs concentrations, reaching maximum degradation (100%) at a concentration of 200 mg ZnONPs.

Discussion

Recently, microbial platforms for the production of nanomaterials as an alternative for the chemical and physical methods are highly recommended owing to their powerful tools for modification, improvement and large-scale production (Dorcheh and Vahabi 2016). Thus, the current study aimed to develop a rapid, easy, cost-effective preparation for zinc oxide nanoparticles (ZnONPs). The fungus *A. tenuissima* AUMC 10624 was grown under submerged fermentation in potato-dextrose broth. The *A. tenuissima* fungal culture (ATCF) was successfully applied for the preparation of ZnONPs. The synthesized nanoparticles were then separated, purified and characterized by different techniques. UV–Vis spectrum of the synthesized ZnONPs exhibited maximum absorption peak at 369 nm, due to its surface plasmon resonance. In accordance with our results, Jamdagni *et al.* (2018) observed the UV spectrum range of ZnONPs is 320–390 nm and the maximum peak at 365 nm. Kalpana *et al.* (2018) observed the UV maxima at 320 nm of ZnONPs synthesized by the *A. niger* ATCC 16404 culture.

X-ray diffraction analysis of the synthesized ZnONPs confirmed the hexagonal crystal structure with space group P63 mc which is in agreement with the Joint Committee on Powder Diffraction Standards (JCPDS) card No. 361451. Moreover, the recorded lattice parameter of ZnONPs was 0·323420 Å which was in agreement with the literature (Abd Elkodous *et al.* 2019). Dynamic light scattering (DLS) analysis showed that the particles size distribution was in the range 10–30. Moreover, the synthesized ZnONPs were monodispersed, as indicated by the PDI value of 0·311. The zeta potential value of the synthesized ZnONPs was −23·92 mV which indicated the high stability of ZnONPs. TEM analyses of the synthesized ZnONPs showed that the particles were spherical in shape and monodispersed. The particle size distribution of the synthesized ZnONPs was in the range 10−30 nm with mean particle size of 15·62 nm which was in a good

agreement with the estimated size from the Scherr equation and DLS analysis. In literature, the size and shape of ZnONPs synthesized by fungi are quite different. For example, Sarkar *et al.* (2014) used *Alternaria alternate* for the synthesis of ZnONPs with spherical, triangular, hexagonal shapes and the particle size distribution range was 45−150 nm. Gao *et al.* (2019) reported that the particle size of ZnONPs synthesized by *A. niger* ranged from 80 to 130 nm and it were almost rod and cluster in shape.

FTIR spectra of the ATCF and the synthesized ZnONPs showed main bands of asymmetric and symmetric vibrations of C-O and C = O bonds in COO^- groups, C-H in CH_2 and in the phenyl ring, bands of phenols and primary amines, bands of O-H in water, which were in a good agreement with literature (Kundu *et al.* 2014; Gao *et al.* 2019). However, the recorded spectrum of the synthesized ZnONPs showed the formation of new absorption band at 618 cm^{-1}. In agreement with our results, Abd Elkodous *et al.* (2019) reported that the absorption peaks recorded at 543 cm^{-1} are corresponding to Zn–O stretching modes. Spectrum of the synthesized ZnONPs further showed the presence of COO^- groups and OH groups which could be attributed to the conjugation of ZnONPs with function groups of the ATCF used in the preparation process. In accordance with these results, Gao *et al.* (2019) observed the presence of the same bands corresponding to COO^- groups and OH groups in the spectrum of ZnONPs synthesized by the cell-free filtrate of *A. niger*. The authors further attributed these observations to the conjugation of ZnONPs with functional groups of the fungal culture. Accordingly, our results suggested that formation of the ZnONPs occurred in two steps; reduction and capping. Firstly, zinc ions were reduced into respective ZnONPs by the active metabolites of the ATCF. Secondly, the synthesized ZnONPs were capped by these metabolites thereby stabilizing them. In literature, several reports concluded that extracellular synthesis of ZnONPs is a nitrate reductase-mediated synthesis, which is responsible for the reduction of Zn ions into ZnONPs (Kundu *et al.* 2014; Chauhan *et al.* 2015; Kalpana *et al.* 2018; Gao *et al.* 2019). The reduction of Zn ions starts through electron transfer from NADH by NADH-dependent reductase that acts as an electron carrier (Hulkoti and Taranath 2014). Thus, Zn-ions obtained electrons and reduced to ZnONPs. Then, the synthesized nanoparticles were capped by the biomolecules of the fungal cultures, thereby stabilizing them (El-Batal *et al.* 2019).

In the present study, the antimicrobial potential of ZnONPs synthesized by the ATCF was evaluated against different multidrug-resistant bacterial strains and three different plant pathogenic fungal species. The obtained results demonstrated a broad spectrum of the antimicrobial properties where all the tested bacterial and fungal strains were inhibited after treatment by ZnONPs. Moreover, the synthesized ZnONPs exhibited potent antimicrobial activity compared to the standard antimicrobials (amoxicillin/clavulanic acid and nystatin). Previous reports have demonstrated the antimicrobial activity of ZnONPs against several bacterial and fungal species; *P. aeruginosa* (Jayaseelan *et al.* 2012; Rajabairavi *et al.* 2017), *Enterococcus* sp., *S. aureus* and *P. mirabilis* (Chauhan *et al.* 2015), *E.coli* and *B. subtilis* (Balraj *et al.* 2017), *S. aureus* and *E. coli* (Khatami *et al.* 2018), *B. subtilis*, *E. coli* and *P. fluorescens* (Jiang *et al.* 2009), *H. pylori* (Saravanan *et al.* 2018), *A. flavus* (Jayaseelan *et al.* 2012), *A. alternata*, *A. niger*, *B. cinerea*, *F. oxysporum* and *P. expansum* (Jamdagni *et al.* 2018), *B. subtilis*, *S. aureus*, *E. faecalis*, *E. coli*, *P. aeruginosa*, *K. pneumoniae*, *C. albicans* and *C. tropicalis* (Abd Elkodous *et al.* 2019; Gao *et al.* 2019). Our results further showed that the estimated MIC value of the synthesized ZnONPs against the tested microbes was in the range of 50–100 μg ml^{-1}. The estimated MIC values of ZnONPs were found to vary in the literature. For example, Khatami *et al.* (2018) showed that the MIC value was 2·0 μg ml^{-1}. Also, Jamdagni *et al.* (2018) concluded the lowest MIC value of 16 μg ml^{-1}. Abd Elkodous *et al.* (2019) showed that the MIC value of 16 μg ml^{-1} against the tested microbes was 25 μg ml^{-1}. Generally, the mechanism of the antimicrobial activity of nanoparticles was attributed to the high efficacy in inhibiting cellular growth as a result of increasing the production of reactive oxygen species (Dutta *et al.* 2012). Additionally, nanoparticles could interact quickly with the cell membrane and the cell wall causing leakage of proteins, genetic materials and minerals thereby causing cell death (Zhang *et al.* 2007).

In the present study, the synthesized ZnONPs caused a concentration-dependent death for all the treated cancer cell lines and the recorded IC_{50} values were 55·76, 18·02 and 16·78, μg ml^{-1} against Hfb-4, MCF-7 and HEp-2 respectively. In accordance with these results, ZnONPs synthesized by *A. niger* significantly inhibited the growth of HepG-2 cancer cells and the recorded IC_{50} was 19·16 μg ml^{-1} (Gao *et al.* 2019). The authors further showed that ZnONPs was not cytotoxic towards the non-cancerous HEK-293 cells at the tested concentrations (μg ml^{-1}). The exact mechanisms involved in the anticancer activity and selectivity of ZnONPs are not yet fully elucidated. However, few studies indicated that cytotoxicity of ZnONPs may be due to the intracellular release of dissolved Zn ions and reactive oxygen species induction (Turney *et al.* 2012). The increase in Zn ions also caused protein activity disequilibrium and oxidative stress, thereby killing the cell (Rasmussen *et al.* 2017). ZnO

nanoparticles, with their unique properties such as easy synthesis, high selectivity, biocompatibility and enhanced cytotoxicity may be a promising anticancer agent (Bisht and Rayamajhi 2016). Thus, the synthesized ZnONPs in this study showed promising anticancer activity against cancer cells with low-toxic effect on the normal cells, thereby it may find application in cancer chemotherapy.

Results of testing the antioxidant activity of the synthesized ZnONPs confirmed the promising antioxidant potential of ZnONPs when compared to ascorbic acid at different concentrations. The free radical scavenging ability of several metal nanoparticles has been reported (Kovacic and Somanathan 2013). This antioxidant potential was mainly due to neutralization and inhibition of the formation of DPPH free radicals(Li *et al.* 2011). Besides, the high surface to volume ratio could enhance the antioxidant activity of metal nanoparticles (Das *et al.* 2013). Our results further indicated that the recorded IC_{50} of the synthesized nanoparticles was 102·31 μg ml^{-1}. In accordance with our results, ZnONPs synthesized by *A. niger* culture filtrate exhibited antioxidant activity in a dose-dependent manner in a concentration range of 5 and 100 mg ml^{-1} when compared with ascorbic acid (Gao *et al.* 2019). The authors further stated that maximum inhibition of (57·74%) was achieved at 100 μg ZnONPs ml^{-1}. Additionally, Abd Elkodous *et al.* (2019) demonstrated the antioxidant activity of the chemically synthesized ZnONPs with 33% inhibition at 25 μg ZnONPs ml^{-1}. Consequently, the recorded antioxidant property of ZnONPs in this study is promising in terms of concentration which will open the way to the application of ZnONPs as a new source of antioxidants.

In the current study, the photocatalytic behaviour of the synthesized ZnONPs was evaluated by dye degradation of MB under sunlight for 20 min. The synthesized ZnONPs successfully degraded the MB dye in a concentration-dependent manner and the complete degradation was achieved on using 200 mg ZnONPs. Recently, metallic nanoparticles have gained considerable attention in the field of catalytic activation of industrial wastes (Khan *et al.* 2019a, 2019b). In the literature, data regarding the photocatalytic activity of ZnONPs synthesized by microbes are rare. Nevertheless, only a few studies in literature studied the photocatalytic behaviour of ZnONPs synthesized by microbes. Tripathi *et al.* (2014) studied photocatalytic activity of ZnONPs synthesized by *Bacillus licheniformis*. Maximum degradation (83%) of MB dye was attained in the presence of ZnONPs under UV-irradiation for 60 min. In addition, Kalpana *et al.* (2018) stated that the bismarck brown dye showed maximum degradation (89%) using 100 μl ZnONPs in the presence of UV light for 72 h. Accordingly, ZnONPs synthesized by the ATCF in this study showed high efficiency in the degradation MB under solar irradiation. Therefore, they can find application in water treatment plants and textile industries.

In summary, ZnONPs were successfully synthesized using culture filtrate of the endophytic fungus *A. tenuissima*. The synthesized ZnONPs were characterized by various techniques. ZnONPs showed strong antimicrobial potential against all the tested plant and human pathogens. The MTT assay confirmed their cytotoxic activity against different forms of cancer cells. ZnONPs further exhibited promising antioxidant activity. The synthesized nanoparticles further showed efficient degradation of the MB dye. Consequently, the synthesized ZnONPs can be better explored in the near future for many medical, agricultural and industrial applications. Current work is in progress to scale up the production of ZnONPs and study the mechanism of their antimicrobial and anticancer activities.

Acknowledgements

We thank Dr Aya M. Kamal and Dr Shaimaa A. Mousa, Assistant Lecturers, Nuclear Research Center, Atomic Energy Authority of Egypt for their sincere help and support.

Conflict of Interest

The authors declare that they have no conflicts of interest.

Ethical approval

This article does not contain any studies with human participants or animals.

References

Abd Elkodous, M., El-Sayyad, G.S., Abdel Maksoud, M.I.A., Abdelrahman, I.Y., Mosallam, F.M., Gobara, M. and El-Batal, A.I. (2019) Fabrication of ultra-pure anisotropic zinc oxide nanoparticles via simple and cost-effective route: implications for UTI and EAC medications. *Biol Trace Elem Res*. https://doi.org/10.1007/s12011-019-01894-1.

Balraj, B., Senthilkumar, N., Siva, C., Krithikadevi, R., Julie, A., Potheher, I.V. and Arulmozhi, M. (2017) Synthesis and characterization of zinc oxide nanoparticles using marine *Streptomyces* sp. with its investigations on anticancer and antibacterial activity. *Res Chem Intermed* **43**, 2367–2376. https://doi.org/10.1007/s11164-016-2766-6.

Bisht, G. and Rayamajhi, S. (2016) ZnO Nanoparticles: a promising anticancer agent. *Nanobiomedicine* **3**, 9. https://doi.org/10.5772/63437.

Chauhan, R., Reddy, A. and Abraham, J. (2015) Biosynthesis of silver and zinc oxide nanoparticles using *Pichia fermentans* JA2 and their antimicrobial property. *Appl Nanosci* **5**, 63–71. https://doi.org/10.1007/s13204-014-0292-7.

Das, D., Nath, B.C., Phukon, P. and Dolui, S.K. (2013) Synthesis of ZnO nanoparticles and evaluation of antioxidant and cytotoxic activity. *Colloids Surf B Biointerfaces* **111**, 556–560. https://doi.org/10.1016/j.colsurfb.2013.06.041.

Dorcheh, S.K. and Vahabi, K. (2016) Biosynthesis of nanoparticles by fungi: large-scale production. In *Fungal Metabolites. Reference Series in Phytochemistry* ed. Mérillon, J.M. and Ramawat, K. Switzerland: Springer International Publishing. https://doi.org/10.1007/978-3-319-19456-1_8-1.

Dutta, R.K., Nenavathu, B.P., Gangishetty, M.K. and Reddy, A.V.R. (2012) Studies on antibacterial activity of ZnO nanoparticles by ROS induced lipid peroxidation. *Colloids Surf B Biointerfaces* **94**, 143–150. https://doi.org/10.1016/j.colsurfb.2012.01.046.

El-Batal, A.I., El-Sayyad, G.S., Mosallam, F.M. and Fathy, R.M. (2019) *Penicillium chrysogenum*-mediated mycogenic synthesis of copper oxide nanoparticles using gamma rays for *in vitro* antimicrobial activity against some plant pathogens. *J Clust Sci*. https://doi.org/10.1007/s10876-019-01619-3.

El-Sayed, E.R., Ahmed, A.S., Hassan, I.A., Ismaiel, A.A. and Karam El-Din, A.A. (2019a) Strain improvement and immobilization technique for enhanced production of the anticancer drug paclitaxel by *Aspergillus fumigatus* and *Alternaria tenuissima*. *Appl Microbiol Biotechnol* **103**, 8923–8935. https://doi.org/10.1007/s00253-019-10129-1.

El-Sayed, E.R., Ahmed, A.S. and Abdelhakim, H.K. (2019b) A novel source of the cardiac glycoside digoxin from the endophytic fungus *Epicoccum nigrum*: isolation, characterization, production enhancement by gamma irradiation mutagenesis and anticancer activity evaluation. *J Appl Microbiol*. https://doi.org/10.1011/JAM.14510.

El-Sayed, E.R., Ismaiel, A.A., Ahmed, A.S., Hassan, I.A. and Karam El-Dinm, A.A. (2019c) Bioprocess optimization using response surface methodology for production of the anticancer drug paclitaxel by *Aspergillus fumigatus* and *Alternaria tenuissima*: enhanced production by ultraviolet and gamma irradiation. *Biocatal Agric Biotechnol* **18**, 100966. https://doi.org/10.1016/j.bcab.2019.01.034.

El-Sayed, E.R., Abdelhakim, H.K. and Ahmed, A.S. (2020a) Solid-state fermentation for enhanced production of selenium nanoparticles by gamma-irradiated *Monascus purpureus* and their biological evaluation and photocatalytic activities. *Bioproc Biosyst Eng*. https://doi.org/10.1007/s00449-019-02275-7.

El-Sayed, E.R., Abdelhakim, H.K. and Zakaria, Z. (2020b) Extracellular biosynthesis of cobalt ferrite nanoparticles by *Monascus purpureus* and their antioxidant, anticancer and antimicrobial activities: yield enhancement by gamma irradiation. *Mater Sci Eng C* **107**, 110318. https://doi.org/10.1016/j.msec.2019.110318.

El-Sayed, E.R., Ahmed, A.S. and Al-Hagar, O.E.A. (2020c) Agro-industrial wastes for production of paclitaxel by irradiated *Aspergillus fumigatus* under solid-state fermentation. *J Appl Microbiol*. (In press). https://doi.org/10.1111/jam.14574

Gao, Y., Anand, M.A.V., Ramachandran, V., Karthikkumar, V., Shalini, V., Vijayalakshmi, S. and Ernest, D. (2019) Biofabrication of zinc oxide nanoparticles from *Aspergillus niger*, their antioxidant, antimicrobial and anticancer activity. *J Clust Sci* **30**, 937–946. https://doi.org/10.1007/s10876-019-01551-6.

Hosseini, M.R. and Sarviab, M.N. (2015) Recent achievements in the microbial synthesis of semiconductor metal sulfide nanoparticles. *Mat Sci Semicon Proces* **40**, 293–301. https://doi.org/10.1016/j.mssp.2015.06.003.

Hulkoti, N.I. and Taranath, T.C. (2014) Biosynthesis of nanoparticles using microbes—a review. *Colloids Surf B Biointerf* **121**, 474–483. https://doi.org/10.1016/j.colsurfb.2014.05.027.

Ismaiel, A.A., Ahmed, A.S., Hassan, I.A., El-Sayed, E.R. and Karam El-Din, A.A. (2017) Production of paclitaxel with anticancer activity by two local fungal endophytes, *Aspergillus fumigatus* and *Alternaria tenuissima*. *Appl Microbiol Biotechnol* **101**, 5831–5846. https://doi.org/10.1007/s00253-017-8354-x.

Jamdagni, P., Khatri, P. and Rana, J.S. (2018) Green synthesis of zinc oxide nanoparticles using flower extract of *Nyctanthes arbor-tristis* and their antifungal activity. *J King Saud Univ-Sci* **30**, 168–75. https://doi.org/10.1016/j.jksus.2016.10.002.

Jayaseelan, C., Rahuman, A.A., Kirthi, A.V., Marimuthu, S., Santhoshkumar, T., Bagavan, A., Gaurav, K., Karthik, L. *et al.* (2012) Novel microbial route to synthesize ZnO nanoparticles using *Aeromonas hydrophila* and their activity against pathogenic bacteria and fungi. *Spectrochim Acta A Mol Biomol Spectrosc* **90**, 78–84. https://doi.org/10.1016/j.saa.2012.01.006.

Jiang, W., Mashayekhi, H. and Xing, B. (2009) Bacterial toxicity comparison between nano- and micro-scaled oxide particles. *Environ Pollut* **157**, 1619–1625. https://doi.org/10.1016/j.envpol.2008.12.025.

Kalpana, V.N., Katarua, B.A.S., Sravania, N., Vigneshwaria, T., Panneerselvam, B. and Rajeswaria, V.D. (2018) Biosynthesis of zinc oxide nanoparticles using culture filtrates of *Aspergillus niger*: antimicrobial textiles and dye degradation studies. *OpenNano* **3**, 48–55. https://doi.org/10.1016/j.onano.2018.06.001.

Khan, S.A., Noreen, F., Kanwal, S., Iqbal, A. and Hussain, G. (2018) Green synthesis of ZnO and Cu doped ZnO nanoparticles from leaf extracts of *Abutilon indicum*, *Clerodendrum infortunatum*, *Clerodendrum inerme* and investigation of their biological and photocatalytic

activities. *Mater Sci Eng C* **82**, 46–59. https://doi.org/10.1016/j.msec.2017.08.071.

Khan, S.A., Arshad, Z., Shahid, S., Arshad, I., Rizwan, K., Sher, M. and Fatima, U. (2019a) Synthesis of TiO2/Graphene oxide nanocomposites for their enhanced photocatalytic activity against methylene blue dye and ciprofloxacin. *Compos B Eng* **175**, 107–120. https://doi.org/10.1016/j.compositesb.2019.107120.

Khan, S.A., Shahid, S., Nazir, M., Kanwal, S., Zaman, S., Sarwar, M.N. and Haroon, S.M. (2019b) Efficient template based synthesis of Ni nanorods by etching porous alumina for their enhanced photocatalytic activities against methyl red and methyl orange dyes. *J Mol Struct* **1184**, 316–323. https://doi.org/10.1016/j.molstruc.2019.02.038.

Khatami, M., Alijani, H.Q., Heli, H. and Sharifi, I. (2018) Rectangular shaped zinc oxide nanoparticles: green synthesis by Stevia and its biomedical efficiency. *Ceram Int* **44**, 15596–15602. https://doi.org/10.1016/j.ceramint.2018.05.224.

Khoobbakht, Z., Mohammadi, M., Mehr, M.R.A., Mohammadghasemi, F. and Sohani, M.M. (2018) Comparative effects of zinc oxide, zinc oxide nanoparticle and zinc-methionine on hatchability and reproductive variables in male Japanese quail. *Anim Reprod Sci* **192**, 84–90. https://doi.org/10.1016/j.anireprosci.2018.02.017.

Kovacic, P. and Somanathan, R. (2013) Nanoparticles: toxicity, radicals, electron transfer, and antioxidants. *Methods Mol Biol* **1028**, 15–35. https://doi.org/10.1007/978-1-62703-475-3_2.

Kundu, D., Hazra, C., Chatterjee, A., Chaudhari, A. and Mishra, S. (2014) Extracellular biosynthesis of zinc oxide nanoparticles using *Rhodococcus pyridinivorans* NT2: multifunctional textile finishing, biosafety evaluation and in vitro drug delivery in colon carcinoma. *J Photochem Photobiol B Biol* **140**, 194–204. https://doi.org/10.1016/j.jphotobiol.2014.08.001.

Li, Y., Li, X., Wong, Y., Chen, T., Zhang, H., Liu, C. and Zheng, W. (2011) The reversal of cisplatin-induced nephrotoxicity by selenium nanoparticles functionalized with 11-mercapto-1-undecanol by inhibition of ROS-mediated apoptosis. *Biomaterials* **32**, 9068–9076. https://doi.org/10.1016/j.biomaterials.2011.08.001.

Ljaz, F., Shahid, S., Khan, S.A., Ahmad, W. and Zaman, S. (2017) Green synthesis of copper oxide nanoparticles using *Abutilon indicum* leaf extract: antimicrobial, antioxidant and photocatalytic dye degradation activities. *Trop J Pharm Res* **16**, 743–753. https://doi.org/10.4314/tjpr.v16i4.2.

Pongtharangkul, T. and Demirci, A. (2004) Evaluation of agar diffusion bioassay for nisin quantification. *Appl Microbiol Biotechnol* **64**, 268–272. https://doi.org/10.1007/s00253-004-1579-5.

Rajabairavi, N., Raju, C.S., Karthikeyan, C., Varutharaju, K., Nethaji, S., Hameed, A.S.H. and Shajahan, A. (2017) Biosynthesis of novel zinc oxide nanoparticles (ZnO NPs) using endophytic bacteria *Sphingobacterium thalpophilum*. In *Recent Trends in Materials Science and Applications* ed. Ebenezar, J. Springer Proceedings in Physics volume 189. Cham: Springer. https://doi.org/10.1007/978-3-319-44890-9_23.

Rasmussen, J.W., Martinez, E., Louka, P. and Wingett, D.G. (2017) Zinc oxide nanoparticles for selective destruction of tumor cells and potential for drug delivery applications. *Expert Opin Drug Deliv* **7**, 1063–1077. https://doi.org/10.1517/17425247.2010.502560.

Saravanan, M., Gopinath, V., Chaurasia, M.K., Syed, A., Ameen, F. and Purushothaman, N. (2018) Green synthesis of anisotropic zinc oxide nanoparticles with antibacterial and cytofriendly properties. *Microb Pathog* **115**, 57–63. https://doi.org/10.1016/j.micpath.2017.12.039.

Sarkar, J., Ghosh, M., Mukherjee, A., Chattopadhyay, D. and Acharya, K. (2014) Biosynthesis and safety evaluation of ZnO nanoparticles. *Bioprocess Biosyst Eng* **37**, 165–171. https://doi.org/10.1007/s00449-013-0982-7.

Shahid, S., Khan, S.A., Ahmad, W., Fatima, U. and Knawal, S. (2018) Size-dependent bacterial growth inhibition and antibacterial activity of Ag-doped ZnO nanoparticles under different atmospheric conditions. *Indian J Pharm Sci* **80**, 173–180. https://doi.org/10.4172/pharmaceutical-sciences.1000342.

Shahid, S., Fatima, U., Sajjad, R. and Khan, S.A. (2019) Bioinspired nanotheranostic agent: zinc oxide; green synthesis and biomedical potential. *Digest J Nanomater Biostruct* **14**, 1023–1031.

Sharma, D., Sharma, S., Kaith, B.S., Rajput, J. and Kaur, M. (2011) Synthesis of ZnO nanoparticles using surfactant free in-air and microwave method. *Appl Surf Sci* **257**, 9661–9672. https://doi.org/10.1016/j.apsusc.2011.06.094.

Tripathi, R.M., Bhadwal, A.S., Gupta, R.K., Singh, P., Shrivastav, A. and Shrivastav, B.R. (2014) ZnO nanoflowers: novel biogenic synthesis and enhanced photocatalytic activity. *J Photochem Photobiol B Biol* **141**, 288–295. https://doi.org/10.1016/j.jphotobiol.2014.10.001.

Turney, T.W., Duriska, M.B., Jayaratne, V., Elbaz, A., O'Keefe, S.J., Hastings, A.S., Piva, T.J., Wright, P.F. *et al.* (2012) Formation of zinc-containing nanoparticles from Zn^{2+} ions in cell culture media: implications for the nanotoxicology of ZnO. *Chem Res Toxicol* **25**, 2057–2066. https://doi.org/10.1021/tx300241q.

Udayabhanu, G, Nagaraju, G., Nagabhushana, H., Basavaraj, R.B., Raghu, G.K., Suresh, D., Rajanaika, H. and Sharma, S.C. (2016) Green, nonchemical route for the synthesis of ZnO superstructures, evaluation of its applications toward photocatalysis, photoluminescence, and biosensing. *Cryst Growth Des* **16**, 6828–6840. https://doi.org/10.1021/acs.cgd.6b00936

Wajiha, Qureshi, N.A. and Afridi, R. (2018) Comparative analysis of egg adapted vaccines and salinomycin against coccidiosis in chicks. *Microb Pathog* **123**, 454–460. https://doi.org/10.1016/J.MICPATH.2018.08.005

Yusof, H.M., Mohamad, R., Zaidan, U.H. and Abdul Rahman, N. (2019) Microbial synthesis of zinc oxide nanoparticles and their potential application as an antimicrobial agent and a feed supplement in animal industry: a review. *J Anim Sci Biotechnol* **10**, 57. https://doi.org/10.1186/s40104-019-0368-z.

Zaki, A.G., El-Shatoury, E.H., Ahmed, A.S. and Al-Hagar, O.E.A. (2019) Production and enhancement of the acetylcholinesterase inhibitor, huperzine A, from an endophytic *Alternaria brassicae* AGF04 1. *Appl Microbiol Biotechnol* **103**, 5867–5878. https://doi.org/10.1007/s00253-019-09897-7

Zhang, L., Jiang, Y., Ding, Y., Povey, M. and York, D. (2007) Investigation into the antibacterial behaviour of suspensions of ZnO nanoparticles (ZnO nanofluids). *J Nanopart Res* **9**, 479–489. https://doi.org/10.1007/s11051-006-9150-1.

Zhao, C.-Y., Tan, S.-X., Xiao, X.-Y., Qiu, X.-S., Pan, J.-Q. and Tang, Z.-X. (2014) Effects of dietary zinc oxide nanoparticles on growth performance and antioxidative status in broilers. *Biol Trace Elem Res* **160**, 361–367. https://doi.org/10.1007/s12011-014-0052-2.